Journal of *Marine Science and Engineering*

MDPI

Article

Three-to-One Internal Resonance of L-Shaped Multi-Beam Structure with Nonlinear Joints

Yunxu Shi [1], Zhe Wu [1], Wei Liu [1] and Jin Wei [1,2,*]

[1] School of Electromechanical and Automotive Engineering, Yantai University, Yantai 264005, China
[2] State Key Laboratory of Mechanics and Control of Mechanical Structures, Nanjing University of Aeronautics and Astronautics, Nanjing 210016, China
* Correspondence: weijin@ytu.edu.cn

Abstract: In this paper, a reduced-order analytical model for an L-shaped multi-beam structure with nonlinear joints is presented to investigate the nonlinear responses of the system with three-to-one internal resonances conditions. Firstly, the global mode shapes are used to obtain an explicit set of nonlinear ordinary differential equations of motion for the system. Then, the first two natural frequencies of the system are calculated to determine the specific tip mass that results in three-to-one internal resonance. Subsequently, an approximation of the analytical solution of the dynamic model with two-degree-of-freedom is derived by using the multi-scale method. The accuracy of the approximation solution is verified by comparing it with the numerical solution obtained from the original motion equations. Based on the nonlinear dynamical model obtained by this paper, the frequency response curves are given to investigate the nonlinear dynamic characteristic of the L-shaped multi-beam structure with nonlinear joints. The results show that the nonlinear stiffness of the joints has a great influence on the nonlinear response of the system with three-to-one internal resonance conditions.

Keywords: L-shaped multi-beam structure; nonlinear joint; multi-scale method; three-to-one internal resonance; nonlinear dynamics

Citation: Shi, Y.; Wu, Z.; Liu, W.; Wei, J. Three-to-One Internal Resonance of L-Shaped Multi-Beam Structure with Nonlinear Joints. *J. Mar. Sci. Eng.* **2022**, *10*, 1461. https://doi.org/10.3390/jmse10101461

Academic Editor: José António Correia

Received: 23 August 2022
Accepted: 6 October 2022
Published: 9 October 2022

1. Introduction

Within the fields of mechanical, aeronautical and civil engineering, L-shaped beams play an increasingly important role, which makes people very interested in their structural and dynamic characteristics. Nowadays, L-shaped beams have been widely used, e.g., L-shaped beams and L-shaped beam frames are often used in building construction, the design of ledges of L-shaped beams, and L-shaped beams are also commonly used in the design of piezoelectric energy harvester and internal structure of acceleration sensors used for earthquake disaster detection. Moreover, they are usually used as a component in space shuttles and the large space structures of flexible manipulators.

At present, the applied research on L-shaped beams can be roughly divided into two categories. Firstly, in the aspect of construction engineering, a typical use of the L-shaped spandrel is on a simple span that supports precast deck elements, such as double-tee beams. Nafadi [1], based on the research findings, proposed an experimental program consisting of full-scale reinforced and pre-stressed concrete L-shaped beams, and to develop comprehensive design guidelines for precast concrete L-shaped beam ledges. Hamzelood, et al. [2] proposed a theoretical model for damage detection of L-shaped beam based on embedded active sensors of piezoelectric plates and used statistical algorithms such as root mean square deviation and cross-correlation to conduct damage detection of L-shaped beam. Rossit, et al. [3] studied an L-shaped beam structure with cracks by analytical method and obtained the natural frequency of plane vibration of the L-shaped beam structure by considering cracks at different positions and depths. Secondly, in mechanical engineering,

L-shaped beams are often used in piezoelectric energy harvesters. In comparison with a simple beam, an L-shaped beam could have internal resonance (by selecting the appropriate dimensions and parameters of the L-shaped beam) and saturation phenomenon. This advantage in nonlinear systems increases the frequency range of energy harvesting, and therefore increases output power from the system. Liu, et al. [4] proved that the frequency range of energy acquisition of an L-shaped beam structure with terminal mass is much larger than that of the cantilever beam. Sharifi Moghaddam, et al. [5] evaluated the energy obtained by nonlinear vibration of the L-shaped beam using piezoelectric plates and obtained the best resistance load and the best effective output power of the system. McCollum, et al. [6] experimentally measured the power transmission in an L-shaped beam and obtained the vibration power transmitted through the joint between two beams forming an L-shaped structure when one beam was excited by the free end force. Finally, L-shaped beams are often used in the internal structure design of acceleration sensors. An acceleration sensor is one of the key points in the field of seismic disaster monitoring and its performance is very important for the monitoring of low-frequency seismic signals. Wang, et al. [7] designed and produced a triple-axis accelerometer with a double L-shaped beam structure, providing an effective manufacturing method for further improving the sensitivity characteristics of the triple-axis accelerometer. Pan, et al. [8] developed an FBG acceleration sensor with symmetric L-beam structure to detect low-frequency seismic signals. A symmetric L-beam is added on the basis of the elastic diaphragm. The L-shaped beam can be regarded as a lever, which can amplify the weak vibration signals well and the symmetric L-shaped beams can improve the sensitivity of the sensor and improve the responsiveness of the sensor during strain transfer.

It can be seen from the above discussion that L-shaped beams have been the subject of a very wide range of research in the field of application, so we should have a more in-depth study of the L-shaped beam. So far, there is little research on three-to-one internal resonance, and most of the previous research was carried out under the condition of 2:1 internal resonance. For example, Balachandran, et al. [9] studied the planar dynamic response of the flexible L-shaped beam-mass structure under the condition of 2:1 internal resonance, and Erturk, et al. [10] proposed to use the L-shaped beam-mass structure as a new piezoelectric harvesting device under the condition of 2:1 internal resonance to improve the possibility of power output in high energy collection. Before these, there have been many studies on three-to-one internal resonance of other beams, such as Char-Ming, [11] et al., who studied the nonlinear plane response of joint beams under the condition of three-to-one internal resonance. Kar, et al. [12] studied the nonlinear behavior of a long thin beam bearing concentrated mass under the excitation of the principal parameter base. By adjusting the size of the beam-mass system and the position of the additional mass, the system showed a three-to-one internal resonance. Tekin, [13] et al. studied the vibration problem of a multi-order beam with cubic nonlinearity under the condition of three-to-one internal resonance and found the general approximate solution to the problem with the multi-scale method. Hegazy [14] studied the nonlinear response of the chord-beam coupling system to parametric excitation under three-to-one internal resonance. The steady-state solution of the system is obtained by solving the frequency response equation numerically, and the influence of different parameters on the system performance is studied. There are also studies on the nonlinear response of curved beams in the case of 1:1 and three-to-one internal resonance [15]. In recent years, the research on three-to-one internal resonance has been further expanded. For example, Garg, et al. [16] conducted a nonlinear dynamic analysis of the piezoelectric energy harvester of a cantilever beam based on parameter-based excitation. By adjusting the additional mass at three-to-one internal resonance, an attempt is made to obtain electrical energy over a wider frequency range. Guillot, et al. [17] obtained experimental and theoretical results of nonlinear dynamics of homogeneous piezoelectric thin beams under the conditions of 2:1 and three-to-one internal resonance by using the same method. Taking the internal resonance of three-to-one as the center, the numerical harmonic balance method is used to solve the governing equation, the periodic solution

of the system under harmonic forcing is obtained, and the energy exchange between the internal resonance modes of three-to-one is observed. Therefore, it is necessary to study the nonlinear dynamic behavior of an L-shaped beam under three-to-one internal resonance to better understand the nonlinear vibration of an L-shaped beam.

In this paper, the beam structure with nonlinear joints is adopted. Firstly, at present many parts of mechanical structure adopt nonlinear joints and the stiffness of nonlinear joints will affect the resonance response of the structure. Pan, et al. [18] considered the influence of nonlinear joint stiffness on the response of the double-jointed system and propose a block mass model to characterize the mechanical properties of bolted flange joints. In addition, in the very popular research field of the manipulator, there are also many studies on the nonlinear joint of the manipulator. Liu, et al. [19] developed a nonlinear model of a special cable in space robotic arms in the space environment. The theoretical findings revealed in this study are significant to future research on the slow rotations and oscillations of weak robot joints in space exploration with robotic arms. Park, et al. [20] proposed a safe joint mechanism (SJM-II)-nonlinear spring system for collision safety. It can simultaneously provide both positioning accuracy and collision safety. So, in this paper, the influence of nonlinear joint on the whole system is also considered in the study of L-shaped beam. Recently, Wei, et al. conducted nonlinear dynamic modeling and analysis on L-shaped beam structure [21] and double-beam structure [22] with terminal mass connected by nonlinear nodes, and this paper conducted corresponding theoretical research on this basis. In addition, the derived low-dimensional high-precision model is also an analytical method to obtain global modes proposed by Wei, et al. [23]. Based on this model, the nonlinear response characteristics under the condition of three-to-one internal resonance are studied by using the multi-scale method.

According to the above, there is little research on the three-to-one internal resonance of an L-shaped beam, so we have conducted some work on this kind of structure. Firstly, the L-shaped multi-beam model with nonlinear joints is established. Then, by applying the dynamic modeling method proposed in the L-shaped beam structure [21], we obtain the nonlinear ordinary differential equation of motion of the system. Next, the modal analysis of the beam structure is carried out, mainly considering the influence of the first two frequencies on the system. Then we make the perturbation analysis of the motion, analyzing the nonlinear dynamics of the L-shaped multi-beam structure under three-to-one internal resonance and considering the primary resonance of the first mode and second mode. Finally, we plot frequency-response curves to describe the nonlinear dynamic phenomenon under the condition of three-to-one internal resonance.

2. Dynamic Model

2.1. Governing Equations of Motion

The L-shaped beam consists of a horizontal beam, a vertical beam, two nonlinear torsional joints, and a rigid body, as shown in Figure 1. The horizontal beam is connected to the support and vertical beams, respectively, through joint S_1 and joint S_2. The coordinate of the horizontal beam with length L_1 is represented by (x_1, y_1), the coordinate of the vertical beam with length L_2 is denoted by (x_2, y_2), and the origin is located at the joint S_1 and S_2, respectively. The L-shaped beam is subjected to the vertical acceleration $Y_0 \cos \Omega t$ and the horizontal acceleration $X_0 \cos \Omega t$, which make the horizontal beam and vertical beam have transverse displacement v_1 and v_2, respectively, where X_0 and Y_0 are the horizontal and vertical peak amplitude of the acceleration, respectively, and Ω is the excitation frequency. The tip mass is located at the end of the vertical beam, m represents the mass of the tip mass, x_m and y_m represent the horizontal and vertical displacement of the tip mass, respectively, which correspond to the displacement v_1 and v_2 of the L-shaped beam structure. We use θ_m to describe the rotational deformation of the tip mass. The coordinates of the tip mass are (x_m, y_m), and the origin is at the center of mass of the tip mass.

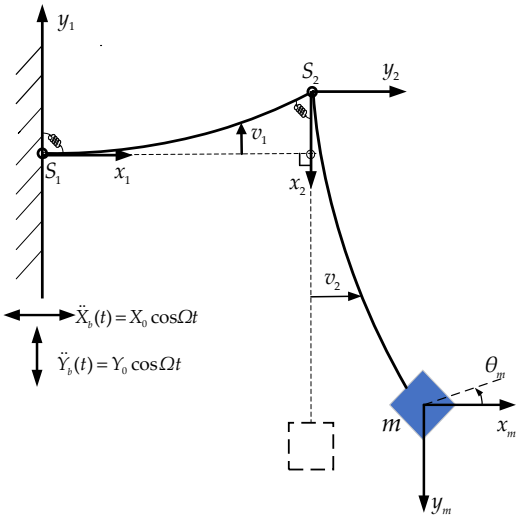

Figure 1. Schematic of L-shaped multi-beam structure.

Considering the external vertical excitation and horizontal excitation, the motion equations of horizontal and vertical beams are derived according to Euler-Bernoulli beam theory.

$$\rho\ddot{v}_i + EIv_i^{''''} + \xi\dot{v}_i + \eta I\dot{v}_i^{''''} = f_i(t), i = 1, 2. \tag{1}$$

where an overdot denotes partial differentiation with respect to time t, a prime denotes partial differentiation with respect to x. It is assumed that the dimensions of the cross-section and material property of the two beams are the same. ρ, E and I represent mass per unit length, elastic modulus and area moment of inertia of the two beams, respectively. The transverse force on the horizontal beam and vertical beam are $f_1 = \rho\ddot{Y}_b$ and $f_2 = \rho\ddot{X}_b$, respectively.

Assuming that the external damping and internal damping are proportional to the mass and stiffness, respectively and they are denoted by ξ and η. They can be expressed as:

$$\xi = a\rho, \eta = bE. \tag{2}$$

where a and b are proportionality constants.

The tip mass and vertical beam can be regarded as attached to the end of the horizontal beam and the governing equation of motion along the x_2-axis is:

$$(\rho L_2 + m)\ddot{y}_m + c_r\dot{y}_m - EIv_1'''(L_1, t) = (\rho L_2 + m)\ddot{Y}_b. \tag{3}$$

where c_r is the damping coefficient of the horizontal beam in the direction of x_2 axis translation, expressed as:

$$c_r = a(\rho L_2 + m). \tag{4}$$

From Figure 2, it can be obtained that the motion equation for the tip mass rotation and translation in horizontal direction are

$$J\ddot{\theta}_m + c_J\dot{\theta}_m + EIv_2''(L_2, t) - \frac{d}{2}EIv_2'''(L_2, t) = 0, \tag{5}$$

$$m\ddot{x}_m + c_m\dot{x}_m - EIv_2'''(L_2, t) = m\ddot{X}_b. \tag{6}$$

where, J represents the moment of inertia of the tip mass, c_J and c_m are the damping of the tip mass for the rotation and translation in horizontal direction, respectively. They are proportional to the tip mass moment of inertia and mass, respectively, so they can be expressed as

$$c_J = aJ, c_m = am. \tag{7}$$

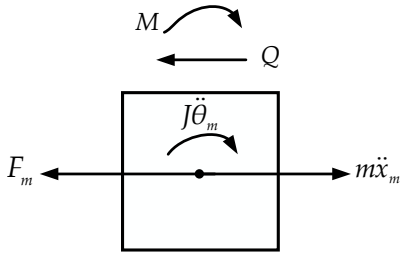

Figure 2. Natural conditions on a rigid body. M is the bending moment of the vertical beam on the rigid body, $M = EIv_2''(L_2, t)$. Q is the shear force of vertical beam on rigid body, $Q = EIv_2'''(L_2, t)$. $F_m = m\ddot{X}_b$ is the external force applied to the rigid body.

For the nonlinear torsional joint, it is described as a massless system with a single degree of freedom nonlinear spring with a damper, as shown in Figure 3. The nonlinear transfer torque formula of the i-th joint can be expressed as:

$$M_i^T = k_L\theta_i + k_N\theta_i^3,\ i = 1, 2. \tag{8}$$

where k_L and k_N are linear stiffness and cubic nonlinear stiffness of nonlinear torsional joint, respectively, θ_i is the torsional deformation of the i-th joint S_i.

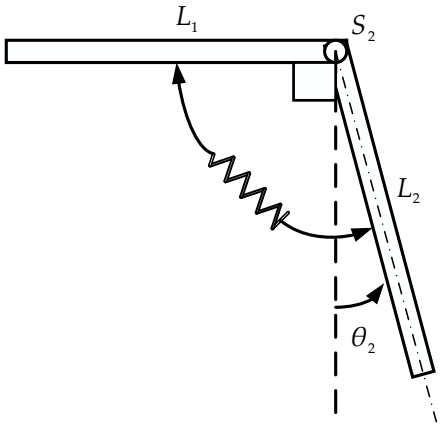

Figure 3. Schematic of joint model.

2.2. Determination of Global Mode Shapes of the L-Shaped Multi-Beam Structure

Firstly, the boundary conditions at the joint S_1 and the matching conditions at the joint S_2 and the tip mas are needed to be analyzed. The boundary conditions at the joint S_1 are

$$v_1(0, t) = 0,\ v_1'(0, t) = \theta_1,\ EIv_1''(0, t) = M_1^T \tag{9}$$

As shown in Figure 4a, the geometric match conditions at the joint S_2 are

$$v_1'(L_1, t) + \theta_2 = v_2'(0, t),\ v_2(0, t) = 0, \tag{10}$$

As shown in Figure 4b, the moment matching boundary conditions at the joint S_2 are

$$EIv_1''(L_1, t) = M_2^T = EIv_2''(0, t). \tag{11}$$

The geometric match conditions of the tip mass are

$$v_1(L_1, t) = y_m,\ v_2(L_2, t) - \frac{d}{2}\theta_m = x_m,\ v_2'(L_2, t) = \theta_m. \tag{12}$$

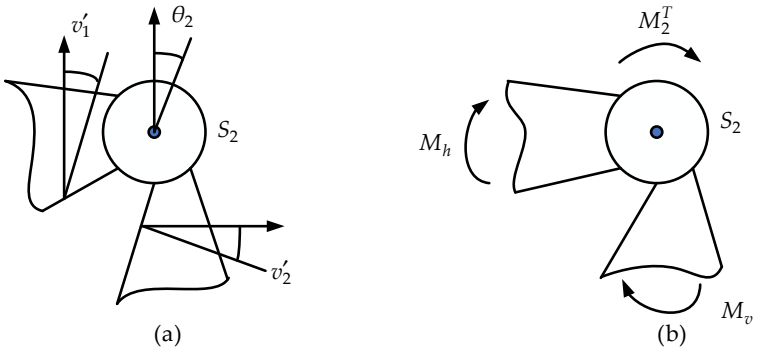

Figure 4. Schematic of (**a**) geometric matching conditions and (**b**) force matching conditions at joint S_1; $v_1' = v_1'(L_1, t)$, $v_2' = v_2'(0, t)$, M_h and M_v are the bending moments acting at the joint, $M_h = EIv_1''(L_1, t), M_v = EIv_2''(0, t)$.

In order to obtain the mode shapes of the L-shaped multi-beam structure, its eigenvalue problem needs to be solved. It is assumed that the displacements of the L-shaped multi-beam jointed structure are separable in space and time by the following forms:

$$v_i(x,t) = \varphi_i(x)e^{j\omega t},\ \theta_i = \Theta_i e^{j\omega t},\ x_m = X_m e^{j\omega t},\ y_m = Y_m e^{j\omega t},\ \theta_m = \Theta_m e^{j\omega t},\ i = 1,2. \quad (13)$$

where ω is an unknown constant corresponding to the natural frequency of the system. By using the separable solution given in Equation (13), the equations of the motion for the beams in Equation (1) without the damping and the external force are transformed into the following form:

$$EI\varphi_i^{\prime\prime\prime\prime}(x) - \omega^2\rho\varphi_i(x) = 0,\ i = 1,2. \quad (14)$$

The solutions of Equation (14) can be written as

$$\varphi_i(x) = A_i\cos(\beta x) + B_i\sin(\beta x) + C_i\cosh(\beta x) + D_i\sinh(\beta x),\ i = 1,2. \quad (15)$$

where $\beta = \left(\frac{\rho\omega^2}{EI}\right)^{1/4}$. Let

$$\psi = [A_1\ \ B_1\ \ C_1\ \ D_1\ \Theta_1\ \ A_2\ \ B_2\ \ C_2\ \ D_2\ \ \Theta_2\ \ X_m\ \ Y_m\ \ \Theta_m]^{\mathrm{T}}. \quad (16)$$

Substituting Equation (15) into the boundary and matching conditions in (9)–(12) and the dynamic equations of the tip mass in (5) and (6), yields

$$H(\omega)\psi = 0. \quad (17)$$

The natural frequencies of the system are denoted in ascending order by $\omega_1,\ \omega_2,\ \cdots$, which are the roots of the frequency equation $\det(H(\omega)) = 0$. Once the natural frequency ω_s is obtained, the eigenvector $\psi^{(s)}$ can be obtained by Equation (17). Then, the s-th global mode shapes for the system can be determined by Equation (15).

2.3. Dynamic Model

The global mode shapes and time-varying modal coordinates are used to represent the displacement of the L-shaped multi-beam structure with nonlinear joint, which can be expressed as:

$$\begin{aligned} &v_i(x_i,t) = \sum_{j=1}^{n}\varphi_{ij}(x_i)q_j(t),\ \theta_i = \sum_{j=1}^{n}\Theta_{ij}q_j(t),\ x_m = \sum_{j=1}^{n}X_m q_j(t),\\ &y_m = \sum_{j=1}^{n}Y_m q_j(t),\ \theta_m = \sum_{j=1}^{n}\Theta_m q_j(t),\ i = 1,2. \end{aligned} \quad (18)$$

where $q_{\mathrm{j}}(t)$ is the modal coordinate of the system.

Substituting Equation (18) into Equations (1), (3), (5) and (6), the nonlinear ordinary differential equation of motion of the system was obtained by applying the Galerkin procedure:

$$M_s\ddot{q}_s(t) + K_s q_s(t) + c_s\dot{q}_s(t) + \sum_{j=1}^{n}\sum_{j=1}^{n}\sum_{j=1}^{n} d^s_{jkr} q_j q_k q_r = f_s(t),\ s = 1, 2, \cdots n. \tag{19}$$

where M_s and K_s are the s-th modal mass and stiffness of the system, respectively and c_s is the s-th modal damping. d^s_{jkr} represents the nonlinear stiffness of the joint. The relevant terms in Equation (19) are given in Appendix A.

3. The Modal Analysis

In this section, the free vibration characteristics of the system with different tip masses are given to study the three-to-one ratio in the first two natural frequencies of the system. Physical parameters of L-shaped multi-beam structure are shown in Table 1.

Table 1. Parameter values of L-shaped multi-beam structure.

Parameter	Value
Mass density ρ (kg/m^3)	7800
Elastic modulus E (GPa)	200
Horizontal beam length L_1 (m)	0.3
Vertical beam length L_2 (m)	0.4
Beam width $b_1 = b_2$ (m)	0.02
Beam thickness $h_1 = h_2$ (m)	0.006
Linear stiffness k_L (N·m/rad)	240

The ratio of the first two natural frequencies is three-to-one when the tip mass is determined. As shown in Figure 5, under different rigid body masses, the first four natural frequencies of L-shaped multi-beam structure are obtained. From Figure 5, it is shows that the third and fourth natural frequencies are much larger than the second nature frequency. The resonance response of the third mode frequency has little effect on the first two modes. Therefore, only the first two modes are taken to calculate the dynamic response of the L-shaped multi-beam structure with nonlinear joints. It can be seen from Figure 5a that the natural frequency decreases gradually with the increase in m, and when $m \approx 1.32$ the second natural frequency is three times that of the first natural frequency. Figure 5b shows the variation in the detuning parameter σ_1 with m, where $\varepsilon\sigma_1 = \omega_2 - 3\omega_1$, ε is a small dimensionless parameter and σ_1 is a tuning parameter.

Next, the nonlinear dynamics of the system with three-to-one internal resonance at $m \approx 1.32$ are analyzed. The parameters of the first two frequencies of $m \approx 1.32$ are shown in Table 2. It can also be seen from Table 2 that the end displacement of the vertical beam is mainly caused by the torsional deformation of the joint.

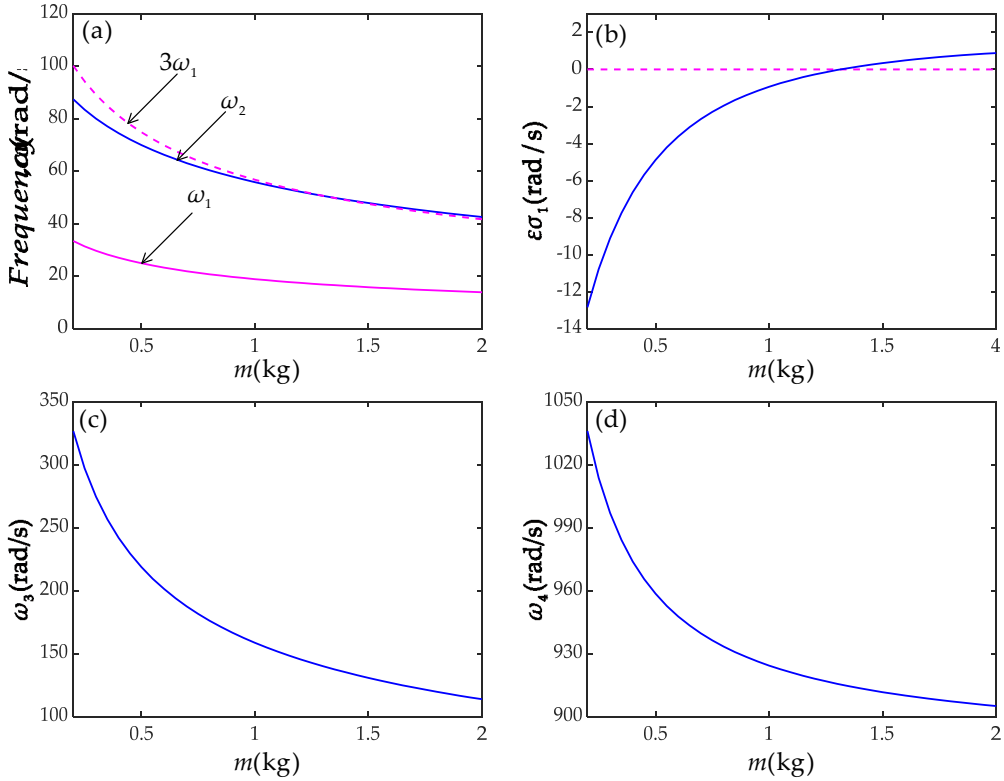

Figure 5. The first four natural frequencies versus tip mass m: (**a**,**b**): the relation between the first two natural frequencies, (**c**): the third natural frequency, (**d**): the fourth natural frequency.

Table 2. Parameter values of the first two frequencies ω(rad/s) when $m \approx 1.32$.

Mode Shape Coefficient	σ = 0.01	
	ω_1 = 16.79	ω_2 = 50.38
The first joint mode displacement Θ_{1j}	−1.15	−3.45
The second joint mode displacement Θ_{2j}	−0.83	3.38
Tip mas horizontal mode displacement X_m	−1.18	0.49
Tip mass vertical mode displacement Y_m	−0.50	−1.20

4. Perturbation Analysis of Motion

In this section, we focus on the nonlinear dynamics of L-shaped multi-beam structure under three-to-one internal resonance. Then, the first two modes are taken to reduce the dynamical model of the L-shaped beam structure to a two degree of freedom nonlinear system. Thus, the nonlinear ordinary differential equations of motion of the system in Equation (19) become

$$\ddot{q}_1 + \omega_1^2 q_1 + 2\hat{\mu}_1 \dot{q}_1 + \hat{\alpha}_{11} q_1^3 + \hat{\alpha}_{12} q_1^2 q_2 + \hat{\alpha}_{13} q_1 q_2^2 + \hat{\alpha}_{14} q_2^3 = \hat{f}_1(t), \tag{20}$$

$$\ddot{q}_2 + \omega_2^2 q_2 + 2\hat{\mu}_2 \dot{q}_2 + \hat{\alpha}_{21} q_1^3 + \hat{\alpha}_{22} q_1^2 q_2 + \hat{\alpha}_{23} q_1 q_2^2 + \hat{\alpha}_{24} q_2^3 = \hat{f}_2(t). \tag{21}$$

where ω_1 and ω_2 are the first and second natural frequencies of the system, respectively. The meanings of all coefficients in Equations (20) and (21) are given in Appendix B.

The multi-scale method is used to analyze the motion of two coupled nonlinear ordinary differential equations. By introducing a time scale $T_n = \varepsilon^n t, n = 0, 1 \ldots$, The first order uniform expansion can be assumed to be:

$$q_1 = q_{10}(T_0, T_1, \ldots) + \varepsilon q_{11}(T_0, T_1, \ldots) + \cdots, \tag{22}$$

$$q_2 = q_{20}(T_0, T_1, \ldots) + \varepsilon q_{21}(T_0, T_1, \ldots) + \cdots. \tag{23}$$

where ε is a small perturbation parameter. The damping coefficient, nonlinearity and force terms are set to the form of the same order as the nonlinear terms.

$$\hat{\mu}_s = \varepsilon\mu_s,\ \hat{\alpha}_{si} = \varepsilon\alpha_{si},\ \hat{f}_s = \varepsilon f_s,\ s = 1,2,\ i = 1,2,3,4. \tag{24}$$

Substituting Equations (22) and (23) into Equations (20) and (21), and balancing coefficients of ε^0 and ε^1 on both sides, we obtain:

ε^0 order

$$D_0 q_{10} + \omega_1^2 q_{10} = 0,\ D_0 q_{20} + \omega_2^2 q_{20} = 0. \tag{25}$$

ε^1 order

$$D_0^2 q_{11} + \omega_1^2 q_{11} = -2D_0(D_1 q_{10} + \mu_1 q_{10}) - \alpha_{11} q_{10}^3 - \alpha_{12} q_{10}^2 q_{20} - \alpha_{13} q_{10} q_{20}^2 - \alpha_{14} q_{20}^3 + f_1(t), \tag{26}$$

$$D_0^2 q_{21} + \omega_2^2 q_{21} = -2D_0(D_1 q_{20} + \mu_2 q_{20}) - \alpha_{21} q_{10}^3 - \alpha_{22} q_{10}^2 q_{20} - \alpha_{23} q_{10} q_{20}^2 - \alpha_{24} q_{20}^3 + f_2(t). \tag{27}$$

The general solution of Equation (25) can be expressed as:

$$q_{10} = A_1(T_1)\exp(i\omega_1 T_0) + cc, q_{20} = A_2(T_1)\exp(i\omega_2 T_0) + cc. \tag{28}$$

where $A_1(T_1)$ and $A_2(T_2)$ are functions to be determined by eliminating the secular terms from q_{11} and q_{21}. Here, cc represents the complex conjugate of the preceding terms.

Next, two cases of the harmonic excitation $\Omega \approx \omega_1$ and $\Omega \approx \omega_2$ are considered. Ω are the frequency of excitation.

4.1. When $\Omega \approx \omega_1$

Here, considering the case of one to three internal resonances and a primary resonance for the first mode. We introduce two detuning parameter σ_1 and σ_2 to quantitatively describe the proximity of ω_2 to $3\omega_1$ and Ω to ω_1. The resonant relations are described as follows:

$$\omega_2 = 3\omega_1 + \varepsilon\sigma_1,\ \Omega = \omega_1 + \varepsilon\sigma_2. \tag{29}$$

By substituting Equations (28) and (29) into Equations (26) and (27) and eliminating the secular terms from q_{11} and q_{21}, the following equations can be obtained.

$$2i\omega_1\left(A_1' + \mu_1 A_1\right) + 3\alpha_{11}A_1^2\overline{A}_1 + 2\alpha_{13}A_2\overline{A}_2 A_1 + \alpha_{12}\overline{A}_1^2 A_2\exp(i\sigma_1 T_1) - \frac{1}{2}X_0\exp(i\sigma_2 T_1) = 0, \tag{30}$$

$$2i\omega_2\left(A_2' + \mu_2 A_2\right) + 2\alpha_{22}A_1\overline{A}_1 A_2 + 3\alpha_{24}A_2^2\overline{A}_2 + \alpha_{21}A_1^3\exp(-i\sigma_1 T_1) = 0. \tag{31}$$

Denoting A_1 and A_2 in polar coordinates.

$$A_1 = \frac{1}{2}a_1(T_1)\exp(i\beta_1),\ A_2 = \frac{1}{2}a_2(T_1)\exp(i\beta_2). \tag{32}$$

Substitute Equation (32) into Equations (30) and (31) and separate the real and imaginary parts of the resulting equations. For the steady-state equation, we get

$$8\omega_1\mu_1 a_1 + \alpha_{12}a_1^2 a_2\sin\gamma_1 - 4f_1\sin\gamma_2 = 0, \tag{33}$$

$$8\omega_2\mu_2 a_2 - \alpha_{21}a_1^3\sin\gamma_1 = 0, \tag{34}$$

$$8\omega_1 a_1\sigma_2 - 3\alpha_{11}a_1^3 - 2\alpha_{13}a_1 a_2^2 - \alpha_{12}a_1^2 a_2\cos\gamma_1 + 4f_1\cos\gamma_2 = 0, \tag{35}$$

$$8\omega_2 a_2(3\sigma_2 - \sigma_1) - 3\alpha_{24}a_2^3 - 2\alpha_{22}a_1^2 a_2 - \alpha_{21}a_1^3\cos\gamma_1 = 0, \tag{36}$$

where $\gamma_1 = \sigma_1 T_1 + \beta_2 - 3\beta_1, \gamma_2 = \sigma_2 T_1 - \beta_1$.

4.2. When $\Omega \approx \omega_2$

Here, considering the case of one to three internal resonances and a primary resonance for the second mode. The resonant relations are described as follows:

$$\omega_2 = 3\omega_1 + \varepsilon\sigma_1, \Omega = \omega_2 + \varepsilon\sigma_2. \tag{37}$$

Applying the procedure in Section 4.1, we can obtain the following four equations:

$$8\omega_1\mu_1 a_1 + \alpha_{12}a_1^2 a_2 \sin\gamma_1 = 0, \tag{38}$$

$$8\omega_2\mu_2 a_2 - \alpha_{21}a_1^3 \sin\gamma_1 - 4f_2 \sin\gamma_2 = 0, \tag{39}$$

$$8\omega_1 a_1(\sigma_1 + \sigma_2) - 9\alpha_{11}a_1^3 - 6\alpha_{13}a_1 a_2^2 - 3\alpha_{12}a_1^2 a_2 \cos\gamma_1 = 0, \tag{40}$$

$$8\omega_2 a_2\sigma_2 - 3\alpha_{24}a_2^3 - 2\alpha_{22}a_1^2 a_2 - \alpha_{21}a_1^3 \cos\gamma_1 + 4f_2 \cos\gamma_2 = 0. \tag{41}$$

where $\gamma_1 = \sigma_1 T_1 + \beta_2 - 3\beta_1, \gamma_2 = \sigma_2 T_1 - \beta_2$.

5. Results Analysis

In this part, we use two methods to calculate the nonlinear response of the system, one is the modulation equations obtained by the multi-scale method, and the other is obtained from Equations (20) and (21) by the numerical method. The accuracy of the approximation solution is verified by compared the results obtained by the two methods. Then, we plot frequency-response curves to describe the nonlinear dynamic phenomenon under the condition of three-to-one internal resonance.

According to Equation (18), the horizontal displacement and vertical displacement of the L-shaped beam structure can be expressed:

$$x_m = \sum_{j=1}^{n} x_m^j = \sum_{j=1}^{n} X_m^j q_j,\ y_m = \sum_{j=1}^{n} y_m^j = \sum_{j=1}^{n} Y_m^j q_j,\ n = 2. \tag{42}$$

where x_m^j and $y_m^j, j = 1, 2$ are j-th displacement of the tip mass.

First of all, we analyze the phenomenon generated when the firs mode primary resonance is performed, namely $\Omega = \omega_1 + \varepsilon\sigma_2$. In these figures, solid blue lines represent stable solutions, while dotted pink lines represent unstable solutions. They are obtained by the modulation equation. The numerical solutions obtained from the original Equations (20) and (21) using the fourth-order Runge-Kutta algorithm are represented by small circles. The unit of k_N values in the figures is N·m/rad^3.

Figures 6 and 7 show the variation in the horizontal and vertical displacement of the L-shaped beam with harmonic excitation Ω when the nonlinear stiffness levels of the joint are $k_N = 1.2 \times 10^4$ N·m/rad^3 and $k_N = 2.4 \times 10^4$ N·m/rad^3, respectively. With the increase in nonlinear stiffness k_N and excitation amplitude F, the horizontal and vertical displacements increase.

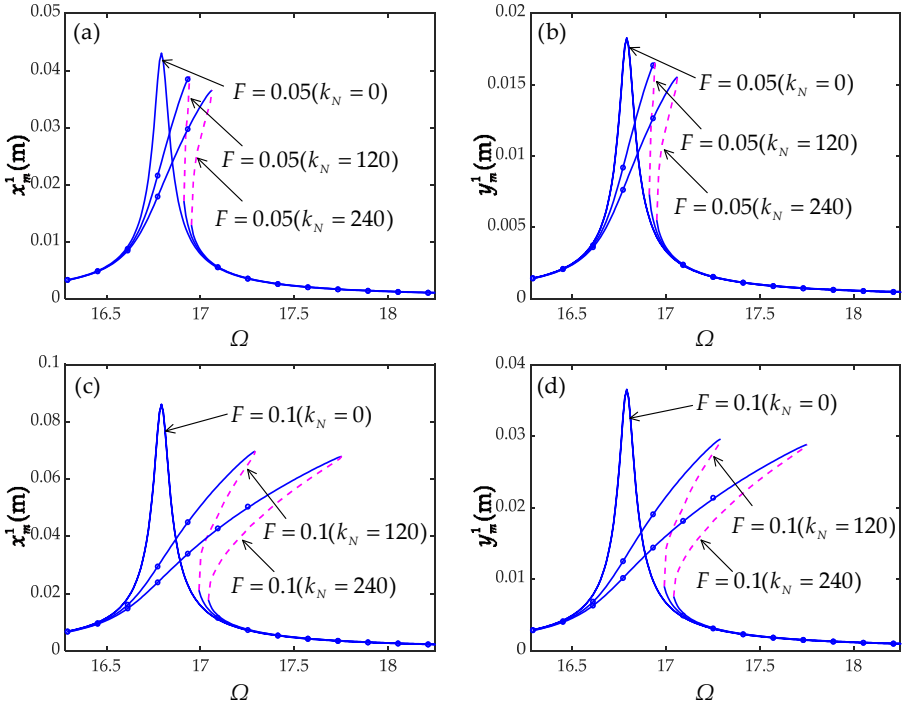

Figure 6. Frequency response curves for the first mode at $\Omega = \omega_1 + \varepsilon\sigma_2$ and $\sigma_1 = 0.01$: (**a**): horizontal displacement for $F = 0.05$, (**b**): vertical displacement for $F = 0.05$, (**c**): horizontal displacement for $F = 0.1$, (**d**): vertical displacement for $F = 0.1$.

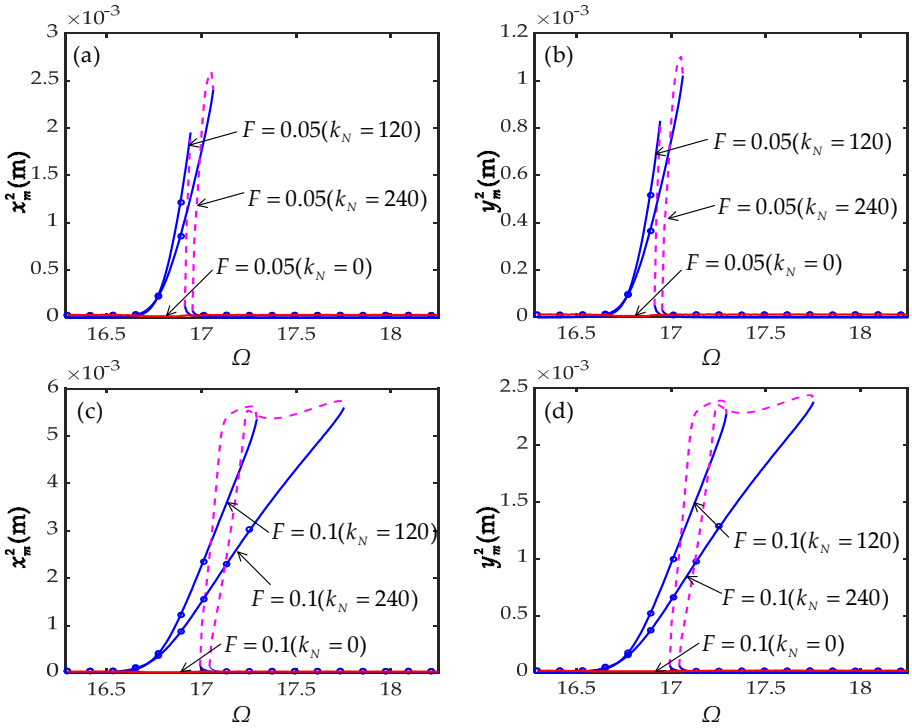

Figure 7. Frequency response curves for the second mode at $\Omega = \omega_1 + \varepsilon\sigma_2$ and $\sigma_1 = 0.01$: (**a**): horizontal displacement for $F = 0.05$, (**b**): vertical displacement for $F = 0.05$, (**c**): horizontal displacement for $F = 0.1$, (**d**): vertical displacement for $F = 0.1$.

By comparing the linear system and nonlinear system, it can be seen from Figure 6 that the linear system ($k_N = 0$) is all stable solutions and without the occurrence of multiple solutions, while the nonlinear system is much more complex. The fundamental difference

between the two is that the transverse value of the frequency corresponding to the peak value of the resonance frequency in the linear system remains unchanged, while the amplitude of the re-resonance frequency in the nonlinear system tends to move to the right with the increase in the excitation amplitude F, so the range of the unstable solution will also become larger.

Figure 7 shows the curve of the displacements x_m^2 and y_m^2 of the tip mass, which is consistent with the change trend of the displacement. The difference is that in a linear system, when the excitation frequency is near the first frequency, the first mode plays a major role, and the second mode cannot be excited. Therefore, the influence of the second mode is very small, so the change trend of the linear system under the second mode is not considered. By comparing the curves of the first mode and the second mode in Figures 6 and 7, it is obvious that the displacements generated in the two modes are very different, and the displacements of the second mode are very small. In order to test whether the displacements generated in the second mode can be ignored, we do the following experiments.

Figure 8 shows the difference in frequency response between 1-dof and 2-dof systems in the case of three-to-one internal resonance. There is only one mode in the one degree of freedom system, that is, the terms containing the second modal coordinate q_2 are removed from Equation (20). For the two degree of freedom system, the influences of two modes on the system are considered, namely, Equations (20) and (21) are quoted. It can be seen from Figure 8 that there is a significant difference between the frequency response of the one-degree-of-freedom system and the two-degree-of-freedom system. Meanwhile, it can also be seen that the difference increases with the increase in excitation amplitude F under the same nonlinear stiffness. With the increase in nonlinear stiffness, the greater the excitation amplitude, the greater the difference will be. This indicates that the coupling of the first two modes is very strong. Although the displacement of the second mode is very small, it will also have a great influence on the overall displacement, so the influence of the second mode cannot be ignored.

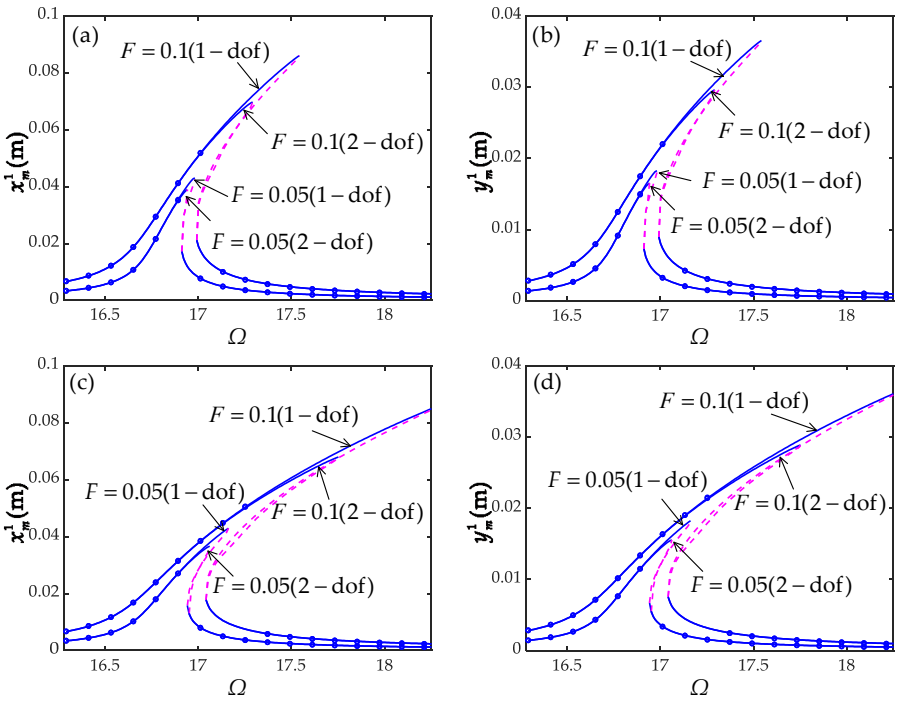

Figure 8. Frequency response curves for the first mode at $\Omega = \omega_1 + \varepsilon\sigma_2$ and $\sigma_1 = 0.01$: (**a**,**b**) $k_N = 1.2 \times 10^4$ N·m/rad^3; (**c**,**d**) $k_N = 2.4 \times 10^4$ N·m/rad^3.

To prove the particularity of the three-to-one internal resonance case, we consider the following case. Figure 9 shows the differences between 1-dof and 2-dof systems in

the frequency-response under different nonlinear stiffness and excitation amplitude when the first two natural frequencies are far away from three-to-one radio. In this case, the results of the 1-dof system are represented by ∘, and the results of the 2-dof system are represented by ∗. The beam length is $L_1 = 0.6$ and $L_2 = 0.2$, respectively, and the first two modes are $\omega_1 = 20.41$ and $\omega_2 = 86.83$, with a ratio of about 4:1. By comparing the case of three-to-one internal resonance, it can be seen that under the same excitation amplitude F, there is the difference only when the value of nonlinear stiffness K_N is very large, even so, the difference of the two cases is very small. From this, it can be concluded that in the case without three-to-one internal resonance, there is little or very weak coupling between the first two modes and it is the first mode that plays a major role.

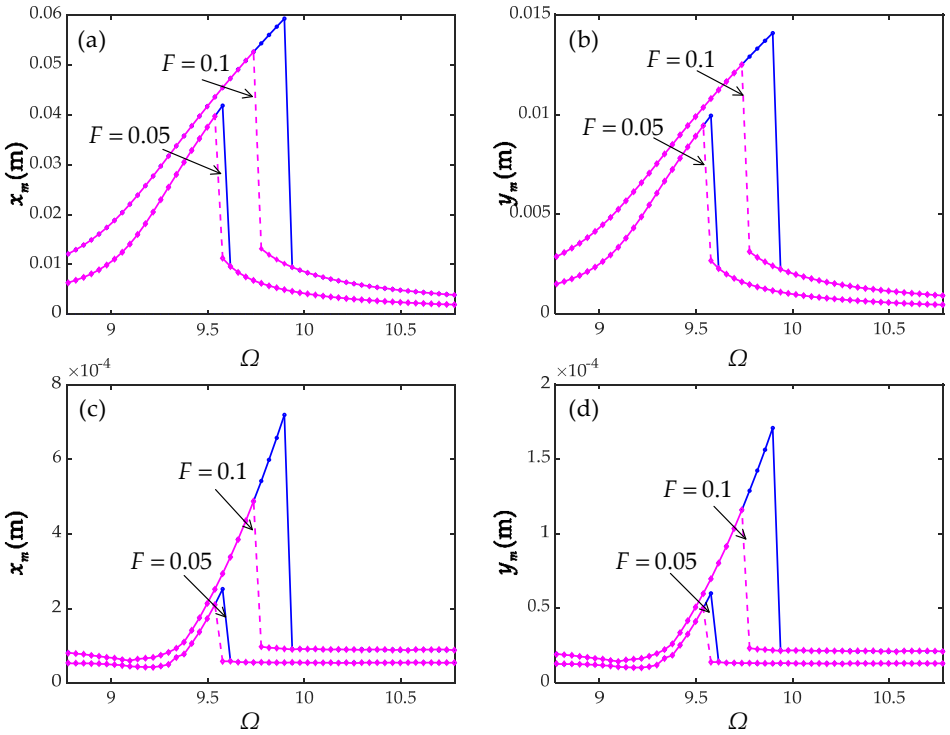

Figure 9. Frequency response curves for the first mode at $\Omega = \omega_1 + \varepsilon\sigma_2$ and $\sigma_1 = 0.01$ without three-to-one internal resonance: (**a**,**b**) $k_N = 1.2 \times 10^4$ N·m/rad^3; (**c**,**d**) $k_N = 2.4 \times 10^4$ N·m/rad^3.

In the frequency response diagrams shown in Figures 10 and 11, it can be seen that the case of the second mode primary resonance is opposite to that of the first mode. In the figure, when the displacement x_m^2 is not zero, the displacement x_m^1 has two cases. The first case is displacement x_m^1 is not zero, we can see that the first order displacement x_m^1 is much larger than its displacement x_m^2. Since internal resonance has the mechanism of transferring energy from high mode to low mode. That means there is resonance occurring inside the system. It can also be said that excitation in the high mode does bring significant response in low order modes. It can also be seen from the figure that when internal resonance occurs, with the increase in excitation amplitude F and nonlinear stiffness k_N of joint, the displacement x_m^2 will increase, and the frequency range causing internal resonance will also increase. In the other case, the displacement x_m^1 is zero. In this case, the result is similar to the result of single degree of freedom. With the increase in excitation amplitude F and nonlinear stiffness k_N of joint, the multi-solution region will become larger.

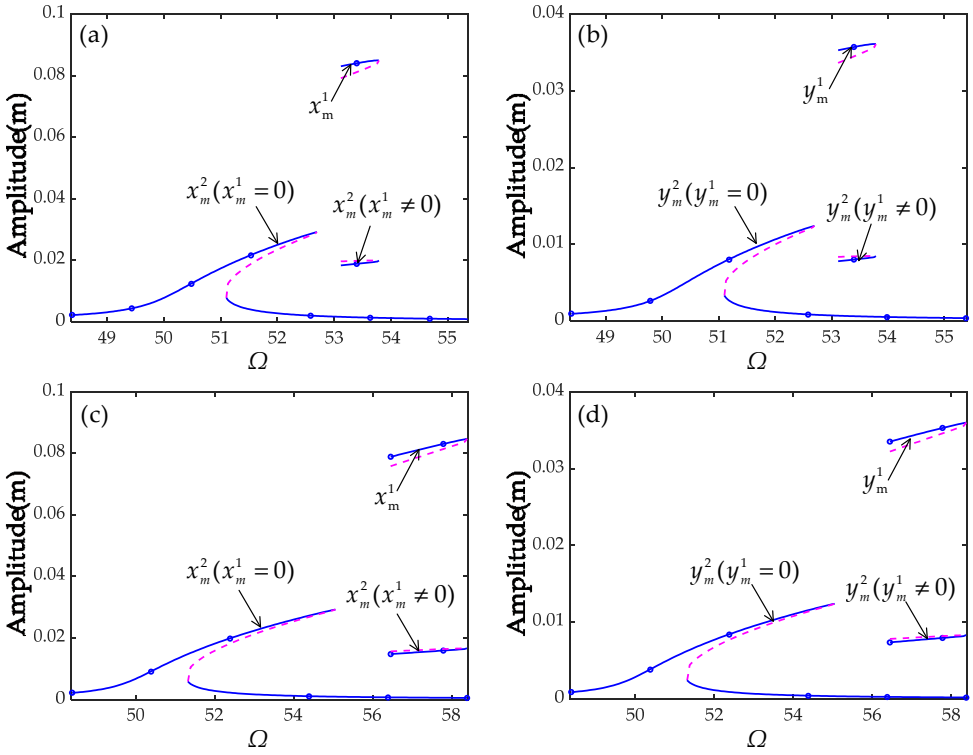

Figure 10. Frequency response curves for the second mode at $\Omega = \omega_2 + \varepsilon\sigma_2$, $\sigma_1 = 0.01$, $F = 0.8$, (**a**,**b**) $k_N = 1.2 \times 10^4$ N·m/rad^3; (**c**,**d**) $k_N = 2.4 \times 10^4$ N·m/rad^3.

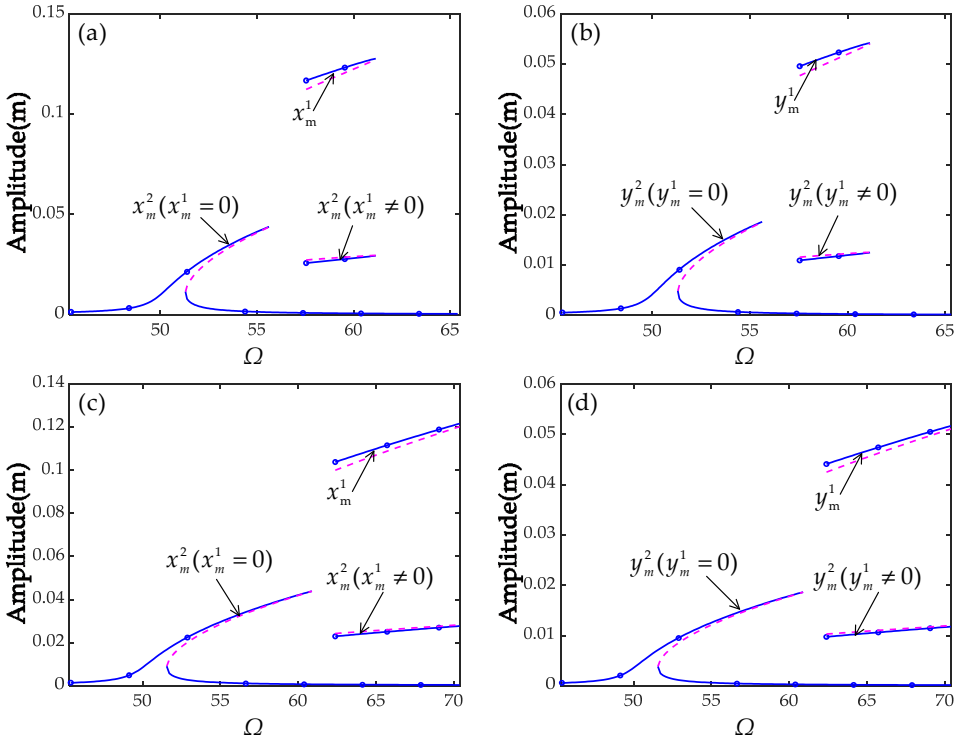

Figure 11. Frequency response curves for the second mode at $\Omega = \omega_2 + \varepsilon\sigma_2$, $\sigma_1 = 0.01$, $F = 1.2$, (**a**,**b**) $k_N = 1.2 \times 10^4$ N·m/rad^3; (**c**,**d**) $k_N = 2.4 \times 10^4$ N·m/rad^3.

6. Conclusions

In this paper, the nonlinear responses of the first two primary resonances of the L-shaped multi-beam structure with nonlinear joints have been investigated analytically

under three-to-one internal resonances condition. The global mode shapes are used to obtain the dynamic model with two-degree-of-freedom. Then, by using the multi-scale method, the approximate analytical solutions of the nonlinear equations are obtained to investigate the influence of the joint nonlinear stiffness on dynamic response behavior of the system.

For the primary resonance of the first mode, when the nonlinear system is under the three-to-one internal resonance condition, the nonlinear stiffness of the joint leads to a very strong coupling effect of the first two modes. Even if the displacement excited by the second mode is very small, its effect on the system cannot be ignored. At the same time, the nonlinear vibration phenomena are also more likely to occur, such as jumping and multiple solutions. When the system is far away from the three-to-one internal resonance conditions, even if the nonlinear stiffness of the joint is large, the effect of the second mode on the system is weak, and it is generally negligible. For the primary resonance of the second mode, the displacement of the system at the excitation frequency away from the second natural frequency may be much greater than those at the excitation frequency near the second natural frequency. At this point, the displacement excited by the first mode is much larger than the displacement excited by the second mode. As the excitation amplitude and joint nonlinear stiffness increase, the excitation frequency in which this occurs is further away from the second natural frequency.

In summary, the nonlinear dynamic model derived in this paper is very suitable for studying the nonlinear dynamic response of the system analytically. Compared with numerical analysis, the approximate analytical solution obtained by analytical method can not only quickly and comprehensively analyze the influence of joint nonlinearity on the nonlinear response of the system, but also better help the design of the joint in such structures.

Author Contributions: Conceptualization, J.W., Z.W. and Y.S.; methodology, J.W. and Y.S.; software, Z.W. and W.L.; investigation, writing—original draft, Y.S. and Z.W.; writing—review and editing, Y.S. and Z.W.; visualization, Z.W. and W.L.; supervision, J.W.; project administration, J.W. and Y.S. All authors have read and agreed to the published version of the manuscript.

Funding: This work was supported by the National Natural Science Foundation of China (Grant No. 12002298), the China Postdoctoral Science Foundation (Grant No. 2020M681578), the Shandong Provincial Natural Science Foundation, China (Grant No. ZR2020QA038).

Institutional Review Board Statement: Not applicable.

Informed Consent Statement: Not applicable.

Data Availability Statement: Not applicable.

Conflicts of Interest: The authors declare no conflict of interest.

Appendix A

The relevant terms in Equation (19)

$$M_s = \rho\left(\int_0^{L_1} {\varphi_{1s}}^2 dx + \int_0^{L_2} {\varphi_{2s}}^2 dx\right) + m{X_{ms}}^2 + (\rho L_2 + m){Y_{ms}}^2 + J{\Theta_{ms}}^2, \tag{A1}$$

$$K_s = EI\left(\int_0^{L_1} {\varphi''_{1s}}^2 dx + \int_0^{L_2} {\varphi''_{2s}}^2 dx\right) + k_L\left({\Theta_{1s}}^2 + {\Theta_{2s}}^2\right), \tag{A2}$$

$$d^s_{jkr} = \frac{1}{M_s}\left\{\begin{array}{l} \int_0^{L_1} \varphi_{1s}\left[\rho\left(\varphi'_{1j}\int_{L_1}^x \int_0^x \varphi'_{1k}\varphi'_{1r}\mathrm{d}x\mathrm{d}x\right)' - (\rho L_2 + m)\varphi''_{1j}\int_0^{L_1}\varphi'_{1k}\varphi'_{1r}dx\right]dx \\ +\int_0^{L_2} \varphi_{2s}\left[\rho\left(\varphi'_{2j}\int_{L_2}^x \int_0^x \varphi'_{2k}\varphi'_{2r}\mathrm{d}x\mathrm{d}x\right)' - m\varphi''_{2j}\int_0^{L_2}\varphi'_{2k}\varphi'_{2r}dx\right]dx \end{array}\right\}, \tag{A3}$$

$$f_s(t) = \frac{1}{M_s}\left\{\ddot{Y}_b\left[\int_0^{L_1}\rho\varphi_{1s}dx + (\rho L_2 + m)Y_{ms}\right] + \ddot{X}_b\left[\int_0^{L_2}\rho\varphi_{2s}dx + mX_{ms}\right]\right\}. \tag{A4}$$

Appendix B

The coefficients lists in Equations (20) and (21) are

$$\hat{\mu}_s = \frac{1}{2}(a + b\omega_s^2),\ \hat{\alpha}_{s1} = \frac{1}{M_s}d_s^{111},\ \hat{\alpha}_{s2} = \frac{1}{M_s}(d_s^{112} + d_s^{121} + d_s^{211}), \tag{A5}$$

$$\hat{\alpha}_{s3} = \frac{1}{M_s}(d_s^{122} + d_s^{212} + d_s^{221}),\ \hat{\alpha}_{s4} = \frac{1}{M_s}d_s^{222},\ \hat{f}_s(t) = \frac{1}{M_s}f_s(t). \tag{A6}$$

References

1. Nafadi, M.K.M. Analytical Modeling and Behavior of Ledges of L-Shaped Beams. Master's Thesis, North Carolina State University, Raleigh, NC, USA, 2013.
2. Hamzeloo, S.R.; Barzegar, M.; Mohsenzadeh, M. Damage Detection of L-shaped Beam Structure with a Crack by Electromechanical Impedance Response: Analytical Approach and Experimental Validation. *Nondestruct. Eval.* **2020**, *39*, 47. [CrossRef]
3. Rossit, C.A.; Bambill, D.V.; Ratazzi, A.R.; Maiz, S. Vibrations of L-shaped beam structures with a crack: Analytical approach and experimental validation. *Exp. Tech.* **2016**, *40*, 1033–1043. [CrossRef]
4. Liu, D.; Al-Haik, M.; Zakaria, M.; Hajj, M.R. Piezoelectric energy harvesting using L-shaped structures. *J. Intell. Mater. Syst. Struct.* **2018**, *29*, 1206–1215. [CrossRef]
5. Sharifi-Moghaddam, S.; Tikani, R.; Ziaei-Rad, S. Energy harvesting from nonlinear vibrations of an L-shaped beam using piezoelectric patches. *J. Braz. Soc. Mech. Sci. Eng.* **2021**, *43*, 158. [CrossRef]
6. McCollum, M.; Gilbert, T.; Rassineux, J.; Cuschieri, J. Experimental measurement of power transmission in an L-shaped beam. *J. Acoust. Soc. Am.* **1987**, *82* (Suppl. S1), S52. [CrossRef]
7. Wang, Y.; Zhao, X.; Wen, D. Fabrication and characteristics of a three-axis accelerometer with double L-shaped beams. *Sensors* **2020**, *20*, 1780. [CrossRef] [PubMed]
8. Pan, J. *Design and Research of FBG Acceleration Sensor with Symmetric L-Beam Structure*; Institute of Disaster Prevention Science and Technology: Langfang, China, 2021.
9. Balachandran, B.; Nayfeh, A. Nonlinear motions of beam-mass structure. *Nonlinear Dyn.* **1990**, *1*, 39–61. [CrossRef]
10. Erturk, A.; Renno, J.M.; Inman, D.J. Piezoelectric energy harvesting from an L-shaped beam-mass structure. In *Proceedings of SPIE, Active and Passive Smart Structures and Integrated Systems 2008*; SPIE: Bellingham, WA, USA, 2008.
11. Chin, C.-M.; Nayfeh, A.H. Three-to-one internal resonances in parametrically excited jointd-clamped beams. *Nonlinear Dyn.* **1999**, *20*, 131–158. [CrossRef]
12. Kar, R.; Dwivedy, S. Non-linear dynamics of a slender beam carrying a lumped mass with principal parametric and internal resonances. *Int. J. Non-Linear Mech.* **1999**, *34*, 515–529. [CrossRef]
13. Tekin, A.; Özkaya, E.; Bağdatli, S. Three-to-one internal resonance in multiple stepped beam systems. *Appl. Math. Mech.* **2009**, *30*, 1131–1142. [CrossRef]
14. Hegazy, U.H. 3:1 Internal resonance of a string-beam coupled system with cubic nonlinearities. *Commun. Nonlinear Sci. Numer. Simul.* **2010**, *15*, 4219–4229. [CrossRef]
15. Emam, S.A.; Nayfeh, A.H. Non-linear response of buckled beams to 1:1 and 3:1 internal resonances. *Int. J. Non-Linear Mech.* **2013**, *52*, 12–25. [CrossRef]
16. Garg, A.; Dwivedy, S.K. Nonlinear dynamics of parametrically excited piezoelectric energy harvester with 1:3 internal resonance. *Int. J. Non-Linear Mech.* **2019**, *111*, 82–94. [CrossRef]
17. Guillot, V.; Givois, A.; Colin, M.; Thomas, O.; Ture Savadkoohi, A.; Lamarque, C.H. Theoretical and experimental investigation of a 1:3 internal resonance in a beam with piezoelectric patches. *J. Vib. Control.* **2020**, *26*, 1119–1132. [CrossRef]
18. Pan, J.; Guan, Z.; Sun, W.; Zeng, Y. Nonlinear oscillations of a dual-joint system involving simultaneous 1:1 and 1:2 internal resonances. *J. Sound Vib.* **2022**, *527*, 116807. [CrossRef]
19. Liu, Y.; Chen, J.; Liu, J.; Jing, X. Nonlinear mechanics of flexible cables in space robotic arms subject to complex physical environment. *Nonlinear Dyn.* **2018**, *94*, 649–667. [CrossRef]
20. Park, J.-J.; Kim, H.-S.; Song, J.-B. Safe robot arm with safe joint mechanism using nonlinear spring system for collision safety. In Proceedings of the 2009 IEEE International Conference on Robotics and Automation, Kobe, Japan, 12–17 May 2009; IEEE: New York, NY, USA, 2009.
21. Wei, J.; Yu, T.; Jin, D.; Liu, M.; Cao, D.; Wang, J. Nonlinear Dynamic Modeling and Analysis of an L-shaped Multi-Beam Jointed Structure with Tip Mass. *Materials* **2021**, *14*, 7279. [CrossRef] [PubMed]
22. Wei, J.; Yu, T.; Jin, D.; Liu, M.; Tian, Y.; Cao, D. Three-to-one internal resonance in a two-beam structure connected with nonlinear joints. *Arch. Appl. Mech.* **2021**, *91*, 3835–3850. [CrossRef]
23. Wei, J.; Cao, D.; Liu, L.; Huang, W. Global mode method for dynamic modeling of a flexible-link flexible-joint manipulator with tip mass. *Appl. Math. Model.* **2017**, *48*, 787–805. [CrossRef]